

# Electronic structures, equilibrium geometries, and finite-temperature properties of $\text{Na}_n$ ( $n=39-55$ ) from first principles

Shahab Zorriasatein,<sup>1,2</sup> Mal-Soon Lee,<sup>1</sup> and D. G. Kanhere<sup>1</sup>

<sup>1</sup>*Department of Physics and Center for Modeling and Simulation, University of Pune, Ganeshkhind, Pune 411 007, India*

<sup>2</sup>*Department of Physics, Islamic Azad University, Tehran South Branch, Tehran 1777613651, Iran*

(Received 9 April 2007; published 12 October 2007)

Density-functional theory has been applied to investigate systematics of sodium clusters  $\text{Na}_n$  in the size range of  $n=39-55$ . A clear evolutionary trend in the growth of their ground-state geometries emerges. The clusters at the beginning of the series ( $n=39-43$ ) are symmetric and have partial icosahedral (two-shell) structure. The growth then goes through a series of disordered clusters ( $n=44-52$ ) where the icosahedral core is lost. However, for  $n \geq 53$ , a three-shell icosahedral structure emerges. This change in the nature of the geometry is abrupt. In addition, density-functional molecular dynamics has been used to calculate the specific heat curves for the representative sizes  $n=43, 45, 48$ , and  $52$ . These results along with already available thermodynamic calculations for  $n=40, 50$ , and  $55$  enable us to carry out a detailed analysis of the heat capacity curves and their relationship with respective geometries for the entire series. Our results clearly bring out strong correlation between the evolution of the geometries and the nature of the shape of the heat capacities. The results also firmly establish the size-sensitive nature of the heat capacities in sodium clusters.

DOI: [10.1103/PhysRevB.76.165414](https://doi.org/10.1103/PhysRevB.76.165414)

PACS number(s): 36.40.Ei, 36.40.Qv, 31.15.Ew, 31.15.Qg

## I. INTRODUCTION

Physics and chemistry of clusters are very active areas of research especially because of the emergence of nanoscience and nanotechnology.<sup>1</sup> Although major efforts have been spent into ground-state investigations, finite-temperature properties are turning out to be very interesting. Such investigations are challenging, both experimentally as well as theoretically. One of the first detailed measurements providing much impetus for theoretical work was on free sodium clusters by Haberland and co-workers.<sup>2-4</sup> These measurements reported the melting temperatures ( $T_m$ ) of sodium clusters in the size range between 55 and 350 and remained unexplained for almost about a decade.

The main puzzle was related to the irregular behavior of the melting temperature and the absence of any correlation between the peaks and the magic numbers either geometric or electronic. A good deal of simulation works has been carried out to explain the sodium data, most of the early work being with classical interatomic potentials.<sup>5-10</sup> It turned out that none of these could obtain qualitative and quantitative agreement with the experimental data. Thus, it needed an *ab initio* density-functional method to achieve this. Indeed, much insight and excellent quantitative agreement have been obtained by density-functional molecular dynamics (DFMD) simulations.<sup>11-20</sup>

Recently, a very different aspect of finite-temperature behavior has been brought out by the experimental and later by theoretical work on gallium clusters.<sup>21,22</sup> The experimental reports of Breaux *et al.*<sup>21</sup> showed that in the size range of  $N=30-55$ , free clusters of gallium melt much above their bulk melting temperature. Interestingly, their experiment also showed that the nature of heat capacity is size sensitive. In fact, addition of even one atom changes the shape of the heat capacity dramatically, e.g., for  $\text{Ga}_{30}$  and  $\text{Ga}_{31}$ . A similar experimental observation has been reported for aluminum clusters in the size range  $n=49-62$ .<sup>23</sup> Such a size-sensitive be-

havior has also been observed in DFMD simulation of  $\text{Au}_{19}$  and  $\text{Au}_{20}$ .<sup>24</sup> A detailed analysis of the ground-state geometries of these clusters brought out the role of order and disorder in their geometries on the shape of the melting curve. A disordered system is shown to display a continuous melting transition leading to a very broad heat capacity curve. However, the effect is subtle and description of order and disorder needs careful qualifications.

In spite of substantial experimental works on sodium clusters over a period of 10 years or so, there is no firm and systematic evidence of size sensitivity. This is mainly due to the fact that the reported experimental data<sup>2-4</sup> are for the size range of  $n=55-350$  at discrete sizes. It is necessary to investigate the effect of addition of few atoms in a continuous manner in appropriate size range. However, it is not clear whether larger clusters having sizes of  $n > 100$  will also show this effect.

An extensive *ab initio* study on the structural properties of small Na clusters up to  $N=20$  has been reported by R othlisberger and Andreoni.<sup>25</sup> The study reveals that pentagonal motifs dominate the structures above  $N=7$ . As expected, most of the atoms in these clusters lie on the surface and a discernible core develops after about  $N=15-16$ . The shapes after these sizes show signature of icosahedral structures. A recent *ab initio* work by Solovyov *et al.* on neutral and singly charged sodium clusters up to  $N=20$  has brought out the importance of many electron correlations for the electronic properties such as ionization potential, multipole moments, and polarizability.<sup>26</sup> There have been several computational studies on finite-temperature properties on sodium clusters using density-functional method. The melting temperature and multipole deformations of  $\text{Na}_{20}$ ,<sup>12</sup>  $\text{Na}_{40}$ ,<sup>11,12</sup> and  $\text{Na}_{55}^+$  (Ref. 12) have been investigated by Rytk onen *et al.* On the basis of 4 ps simulation time, they found the dominant deformation at the liquid phase for  $\text{Na}_{20}$  and  $\text{Na}_{40}$  to be octupole type. Electronically magic clusters  $\text{Na}_{57}^-$ ,  $\text{Na}_{59}^+$ , and  $\text{Na}_{93}^+$  have also been studied by Manninen *et al.*<sup>13</sup> These

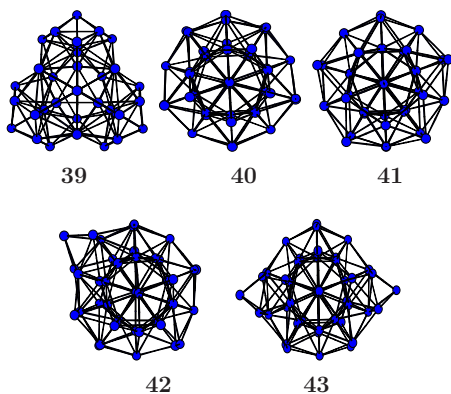


FIG. 1. (Color online) The ground-state geometries of  $\text{Na}_n$  ( $n=39-43$ ).

clusters stay magic through the melting region. Orbital free density-functional calculations have been reported to understand and explain the melting behavior of sodium clusters with different sizes.<sup>27-29</sup>

A systematic study of the finite-temperature behavior of sodium clusters in the size range of  $n=8-55$  has been reported by Lee *et al.*<sup>15</sup> The study reveals that it is not easy to discern any melting peaks below  $n=25$ . However, the simulation data available at rather coarse sizes above  $n=40$  already show size-sensitive feature. In addition to this feature, our recent investigation<sup>20</sup> on  $\text{Na}_{57}$  and  $\text{Na}_{58}$  does bring out the role of geometry and electronic structure on the melting. Nevertheless, in order to draw definitive conclusions, it is necessary to investigate the effect of addition of a few atoms in a continuous manner in appropriate size range. Therefore, we have chosen the size range of  $n=39-55$  and have carried out detailed density-functional investigations. The purpose of the present work is twofold. First is to obtain reliable equilibrium geometries for all the clusters in the size range of  $n=39-55$  and to discern evolutionary trends. We note that  $\text{Na}_{40}$  has a symmetric partially icosahedron core and  $\text{Na}_{55}$  is a complete icosahedron. Thus, it is of considerable interest to examine the growth pattern from  $n=39$  to  $n=55$ . The second purpose is to seek correlation between the nature of the ground state and the evolutionary trends observed in the nature of their specific heats. Toward this end, we have carried out extensive finite-temperature simulations on representative clusters of size  $n=43, 45, 48$ , and  $52$ . Together with the already published results, this gives us access to specific heats for  $\text{Na}_{40}, \text{Na}_{43}, \text{Na}_{45}, \text{Na}_{48}, \text{Na}_{50}, \text{Na}_{52}$ , and  $\text{Na}_{55}$ , a reasonable representation across the series under investigation. Finally, we note that all the DFMD simulations reported so far have yielded excellent agreement with the experimental data.<sup>14,16,20</sup> These reports demonstrate the reliability of density-functional molecular dynamics in describing the finite-temperature properties.

The plan of the paper is as follows. In the next section (Sec. II), we note the computational details. Section III presents equilibrium geometries and their shape systematic. Section IV presents the finite-temperature behavior of  $\text{Na}_{43}, \text{Na}_{45}, \text{Na}_{48}$ , and  $\text{Na}_{52}$ , and finally we discuss the correlation between the ground states and the nature of the specific heats for all the available thermodynamics data. We conclude our discussion in Sec. V.

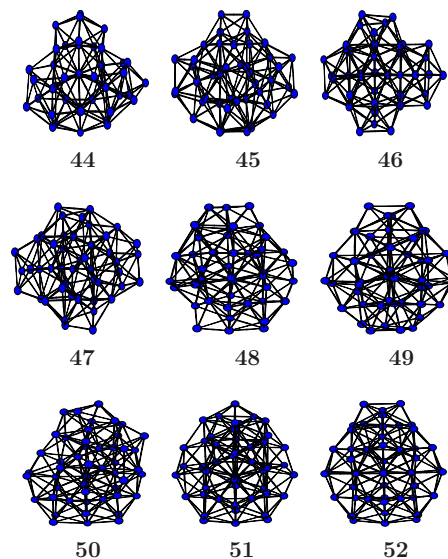


FIG. 2. (Color online) The ground-state geometries of  $\text{Na}_n$  ( $n=44-52$ ).

## II. COMPUTATIONAL DETAILS

We have carried out Born-Oppenheimer molecular dynamics (BOMD) simulations<sup>30</sup> using Vanderbilt's ultrasoft pseudopotentials<sup>31</sup> within the local-density approximation, as implemented in the VASP package.<sup>32</sup> We have optimized about 300 geometries for each of the sodium clusters in the size range between  $n=39$  and  $n=55$ . The initial configuration for the optimization of each cluster was obtained by carrying out a constant temperature dynamics simulation of 60 ps each at various temperatures between 300 and 400 K. For many of the geometries, we have also employed basin hopping<sup>33</sup> and genetic<sup>34,35</sup> algorithms using the Gupta potential<sup>5</sup> for generating initial guesses. Then, we optimized these structures by using the *ab initio* density-functional method.<sup>36</sup> For computing the heat capacities, the isokinetic BOMD calculations were carried out at 14 different temperatures for each cluster of  $\text{Na}_{43}, \text{Na}_{45}, \text{Na}_{48}$ , and  $\text{Na}_{52}$  in the range between 100 and 460 K, each with the time duration of 180 ps or more. Thus, it results in the total simulation time of 2.5 ns per system. In order to get converged heat capacity curve especially in the region of coexistence, more temperatures were required with longer simulation times. We have discarded at least the first 30 ps for each temperature for thermalization. To analyze the thermodynamic properties, we first calculate the ionic specific heat by using the multiple histogram (MH) technique.<sup>37,38</sup> We extract the classical ionic density of states  $[\Omega(E)]$  of the system, or equivalently the classical ionic entropy,  $S(E)=k_B \ln \Omega(E)$ , following the MH technique. With  $S(E)$  in hand, one can evaluate thermodynamic averages in a variety of ensembles. We focus in this work on the ionic specific heat. In the canonical ensemble, the specific heat is defined as usual by  $C(T)=\partial U(T)/\partial T$ , where  $U(T)=\int E p(E, T) dE$  is the average total energy. The probability of observing an energy  $E$  at a temperature  $T$  is given by the Gibbs distribution  $p(E, T)=\Omega(E)\exp(-E/k_B T)/Z(T)$ , with  $Z(T)$  the normalizing canonical partition

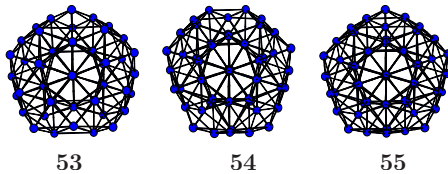


FIG. 3. (Color online) The ground-state geometries of  $\text{Na}_n$  ( $n=53-55$ ).

function. We normalize the calculated canonical specific heat by the zero-temperature classical limit of the rotational plus vibrational specific heat, i.e.,  $C_0=(3N-6)k_B$ .<sup>29</sup>

We have calculated a number of thermodynamic indicators such as root-mean-square bond length fluctuations ( $\delta_{\text{rms}}$ ), mean square displacements (MSDs), and radial distribution function [ $g(r)$ ]. The  $\delta_{\text{rms}}$  is defined as

$$\delta_{\text{rms}} = \frac{2}{N(N-1)} \sum_{i>j} \frac{(\langle r_{ij}^2 \rangle_t - \langle r_{ij} \rangle_t^2)^{1/2}}{\langle r_{ij} \rangle_t}, \quad (1)$$

where  $N$  is the number of atoms in the system,  $r_{ij}$  is the distance between atoms  $i$  and  $j$ , and  $\langle \cdots \rangle_t$  denotes a time average over the entire trajectory. MSD for individual atoms is another traditional parameter used for determining phase transition and is defined as

$$\langle \mathbf{r}_I^2(t) \rangle = \frac{1}{M} \sum_{m=1}^M [\mathbf{R}_I(t_{0m} + t) - \mathbf{R}_I(t_{0m})]^2, \quad (2)$$

where  $\mathbf{R}_I$  is the position of the  $I$ th atom and we average over  $M$  different time origins  $t_{0m}$  spanning over the entire trajectory. The interval between the consecutive  $t_{0m}$  for the average was taken to be about 1.5 ps. The MSDs of a cluster indicate the displacement of atoms in the cluster as a function of time. The  $g(r)$  is defined as the average number of atoms within the region between  $r$  and  $r+dr$ .

We have also calculated the shape deformation parameter ( $\varepsilon_{\text{def}}$ ) to analyze the shape of the ground state for all the clusters.  $\varepsilon_{\text{def}}$  is defined as

$$\varepsilon_{\text{def}} = \frac{2Q_x}{Q_y + Q_z}, \quad (3)$$

where  $Q_x \geq Q_y \geq Q_z$  are the eigenvalues, in descending order, of the quadrupole tensor

$$Q_{ij} = \sum_I R_{iI} R_{jI}. \quad (4)$$

Here,  $i$  and  $j$  run from 1 to 3,  $I$  runs over the number of ions, and  $R_{iI}$  is the  $i$ th coordinate of ion  $I$  relative to the center of mass of the cluster. A spherical system ( $Q_x=Q_y=Q_z$ ) has  $\varepsilon_{\text{def}}=1$  and larger values of  $\varepsilon_{\text{def}}$  indicate deviation of the shape of the cluster from sphericity.

### III. GEOMETRIES

The lowest-energy geometries of sodium clusters ( $\text{Na}_n$ ,  $n=39-55$ ) are shown in Fig. 1 ( $n=39-43$ ), Fig. 2 ( $n$

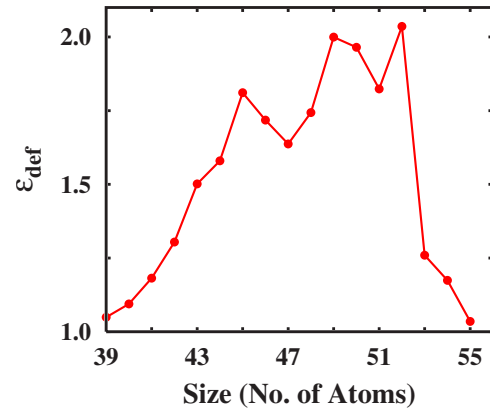


FIG. 4. (Color online) The shape deformation parameter for  $\text{Na}_n$  ( $n=39-55$ ) as a function of cluster size for the ground states.

$=44-52$ ), and Fig. 3 ( $n=53-55$ ). We have also plotted the shape deformation parameter  $\varepsilon_{\text{def}}$  and the eigenvalues of quadrupole tensor for the ground-state geometries of these clusters in Figs. 4 and 5, respectively.

It is convenient to divide these clusters into three groups. The clusters in the first group, shown in Fig. 1, are nearly spherical. The ground-state geometry for  $\text{Na}_{39}$  is highly symmetric. This structure has three identical units, each based on the icosahedral motive and these three units are arranged as shown in Fig. 1. It is interesting to note that an addition of an extra atom changes the structure dramatically. It can be seen that the geometry of  $\text{Na}_{40}$  is based on icosahedral structure with missing 12 corner atoms and (111) facet as reported by Rytkönen *et al.*<sup>11</sup> An extra atom added to this structure is accommodated near the surface and deforms the structure slightly. In addition to the deformation, the distance between the two shells is reduced by 0.3 Å as compared to that in  $\text{Na}_{40}$ . A single atom added to  $\text{Na}_{41}$  is not accommodated in the structure; instead, it caps the surface. However, the low-lying geometries for  $\text{Na}_{42}$  have a spherical shape without any cap (figure not shown). The lowest-energy structure of  $\text{Na}_{43}$

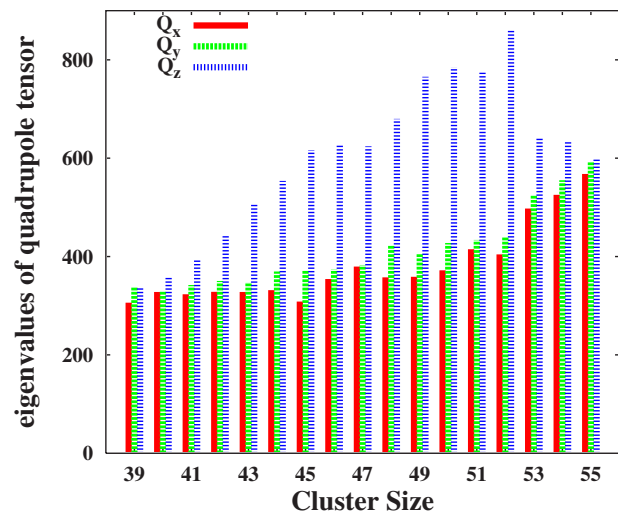


FIG. 5. (Color online) The eigenvalues of the quadrupole tensor for  $\text{Na}_n$  ( $n=39-55$ ) as a function of cluster size for the ground states.

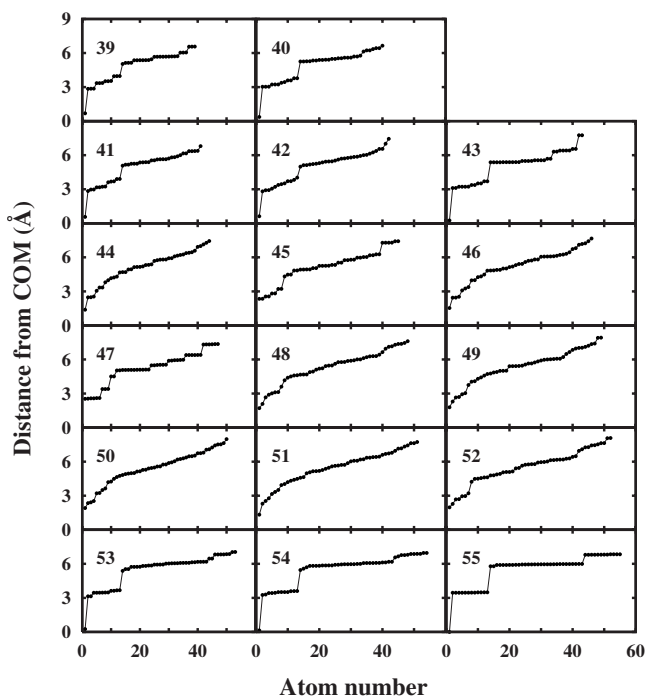


FIG. 6. The distance from the center of mass for each of the atoms ordered in the increasing fashion for the ground states of  $\text{Na}_n$  ( $n=39-55$ ). The formation of the shells is evident from the sharp steps.

shows two caps symmetrically placed on the opposite sides of  $\text{Na}_{41}$ , accompanied by distortion of the icosahedral core. The second group in Fig. 2 consisting of the clusters with  $n=44-52$  shows substantial distortion of the icosahedral core and even loss of this core structure. These clusters essentially represent the transition region from the two-shell icosahedron,  $\text{Na}_{40}$ , to three-shell complete icosahedron,  $\text{Na}_{55}$ .

It can be seen that by adding one atom to  $\text{Na}_{43}$ , the two-shell core is destroyed. The growth from  $n=44$  to  $n=52$  shows successive stages of capping followed by rearrangement in the inner core. There is a dramatic change in the structure as soon as we add one more atom to  $\text{Na}_{52}$ . All the atoms rearrange to form an icosahedral structure as seen in  $\text{Na}_{53}$ . Thus, the clusters in the last group, namely,  $\text{Na}_{53}$  and  $\text{Na}_{54}$ , differ from a perfect icosahedron of  $\text{Na}_{55}$  by an absence of two and one atom(s), respectively (Fig. 3).

The nature of the changes in the shape of the clusters during the growth can be seen in Figs. 4 and 5. The shape deformation parameter ( $\epsilon_{def}$ ) increases to a value about 2 up to  $\text{Na}_{52}$  with slightly higher values for  $\text{Na}_{45}$  and  $\text{Na}_{49}$  (Fig. 4). However, this value drops suddenly for  $\text{Na}_{53}$ . It is interesting to examine the three eigenvalues of quadrupole tensor ( $Q_x, Q_y, Q_z$ ) shown in Fig. 5. It can be seen that two of the eigenvalues are nearly the same up to  $\text{Na}_{52}$ , while the third one continuously grows and indicates that the growth dominantly takes place along one of the directions. A prolate configuration has  $Q_z \gg Q_x \approx Q_y$ . Thus, the majority of the clusters in the second group are prolate. The formation, the destruction, and reformation of the shell structure are clearly seen in Fig. 6. In this figure, we have plotted the distance of each atom from the center of mass arranged in an increasing

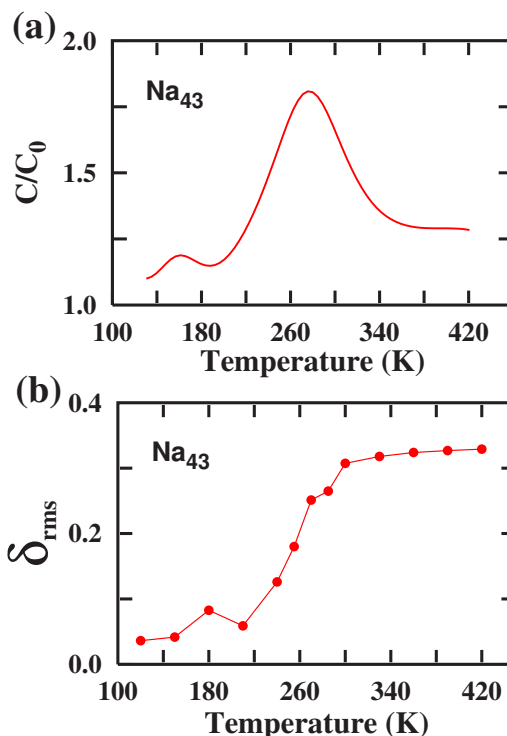


FIG. 7. (Color online) (a) The normalized heat capacity and (b) the  $\delta_{rms}$  for  $\text{Na}_{43}$ . The peak in heat capacity curve is at 280 K.

fashion. Clearly, small rearrangement of atoms yields a change in the structure from  $\text{Na}_{39}$  to  $\text{Na}_{40}$ . The two-shell structures are observed until  $\text{Na}_{43}$ . The formation of the shell structure is reflected in the formation of the sharp steps in the graph. As the size increases from  $\text{Na}_{43}$  to  $\text{Na}_{44}$ , the shell structure is destroyed and seen again at  $\text{Na}_{53}$ . Thus, three shells begin to emerge at  $\text{Na}_{53}$ .

#### IV. THERMODYNAMICS

We have calculated the ionic heat capacity and indicators such as MSDs and root-mean-square bond length fluctuations ( $\delta_{rms}$ ) for four of the representative clusters in the investigated series which are  $\text{Na}_{43}$ ,  $\text{Na}_{45}$ ,  $\text{Na}_{48}$ , and  $\text{Na}_{52}$ .

We note that the thermodynamics of  $\text{Na}_{40}$ ,<sup>11,15</sup>  $\text{Na}_{50}$ ,<sup>15</sup> and  $\text{Na}_{55}$  (Refs. 14 and 16) has already been reported. Thus, it is possible to examine and analyze the systematic variations in the melting characteristic and correlate them with the equilibrium geometries across the entire range of sizes from 40 to 55. The heat capacity and  $\delta_{rms}$  for  $\text{Na}_{43}$  are shown in Figs. 7(a) and 7(b), respectively. We also show typical low-energy geometries (isomers) for  $\text{Na}_{43}$  in Fig. 8. The first isomer shown in Fig. 8(a) has two atoms closest to each other capping the surface and second isomer shows a distorted shape and has no caps. The heat capacity shows a weak peak around 160 K, while the main peak occurs at 280 K. An examination of the motion of ionic trajectory seen as a movie indicates that isomerization [Fig. 8(a)] is responsible for the weak peak.

It is interesting to observe the changes of radial distribution function (RDF) as a function of temperature, as shown

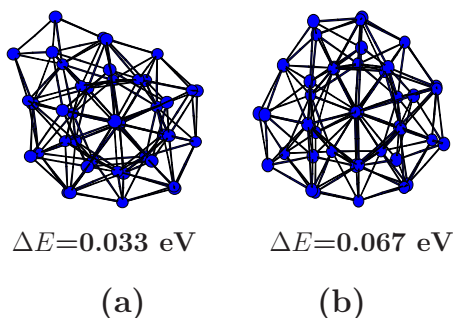


FIG. 8. (Color online) Two low-lying isomers of  $\text{Na}_{43}$ .  $\Delta E$  represents the energy difference with respect to the ground state.

in Fig. 9. At low temperatures, the shell structure is clearly evident. The patterns seen at 180 and 210 K are mainly due to the fluctuation of the cluster between the ground-state and low-lying states. At 300 K and above, the RDF shows the typical melting behavior of a cluster. The  $\delta_{\text{rms}}$  in Fig. 7(b) shows the effect of isomerization around 160 K. It can be seen that the melting region is of the order of 60 K.

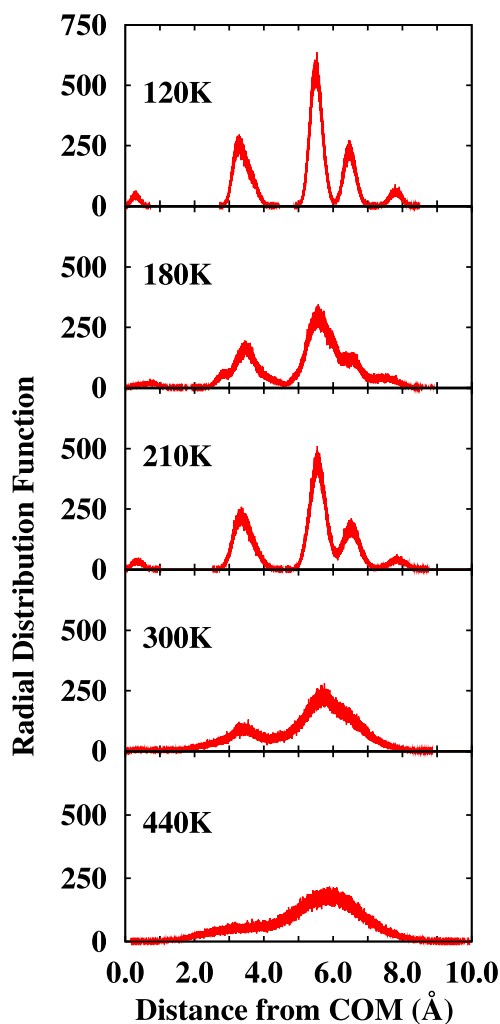


FIG. 9. (Color online) The radial distribution function in arbitrary unit calculated for  $\text{Na}_{43}$  at five different temperatures.

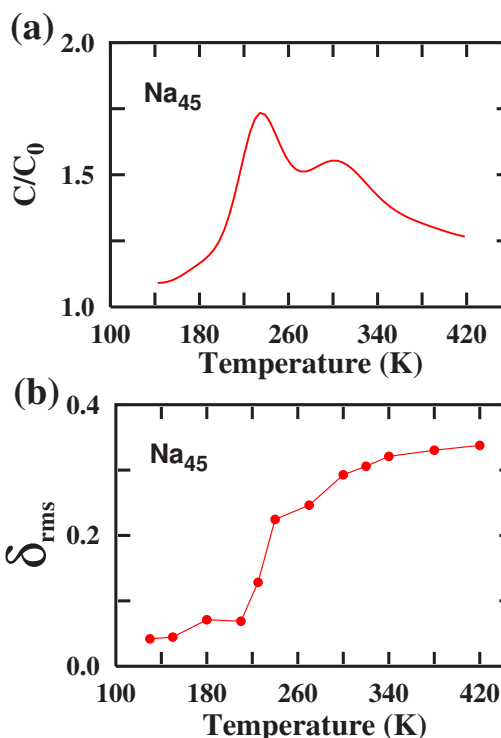


FIG. 10. (Color online) (a) The normalized heat capacity and (b) the  $\delta_{\text{rms}}$  for  $\text{Na}_{45}$ . The heat capacity curve shows a two stage melting process.

Let us recall that  $\text{Na}_{45}$ ,  $\text{Na}_{48}$ , and  $\text{Na}_{52}$  belong to the second class of disordered clusters. Among these,  $\text{Na}_{45}$  shows some signature of partial shells. The heat capacity and  $\delta_{\text{rms}}$  for  $\text{Na}_{45}$  are shown in Figs. 10(a) and 10(b), respectively. The heat capacity of  $\text{Na}_{45}$  shows a first peak around 230 K and a second peak around 300 K. We also show the MSDs of individual atoms at 210 and 225 K in Figs. 11(a) and 11(b), respectively. We have observed the ionic trajectories as a movie in the temperature at 225 K. It turns out that about one-third of atoms in the cluster “melt” at this temperature. This is brought out by the contrasting behavior of the MSDs as shown in Figs. 11(a) and 11(b). Interestingly, all these 15 atoms are on the surface, indicating that surface melting takes place first. The peak around 225 K in the heat capacity is due to partial melting of these surface atoms. We show the  $\delta_{\text{rms}}$  as a function of the temperature in Fig. 10(b). There is a sharp increase in  $\delta_{\text{rms}}$  around 210 K and a slow rise after 240 K, consistent with the behavior of the heat capacity. Thus, in  $\text{Na}_{45}$ , melting takes place in two stages over the range of 120 K.

The heat capacity,  $\delta_{\text{rms}}$ , and  $\epsilon_{\text{def}}$  for  $\text{Na}_{48}$  and  $\text{Na}_{52}$  are shown in Fig. 12. The heat capacity of  $\text{Na}_{48}$  is very broad, indicating almost continuous phase change beginning around 150 K [Fig. 12(a)]. Thus, it is difficult to identify a definite melting temperature. A similar behavior in the heat capacity is also seen for  $\text{Na}_{52}$  except for the small peak in 180 K. This peak is due to the isomerization involving at least the first six isomers (see Fig. 14). It is interesting to note that  $\delta_{\text{rms}}$  for both the clusters also show a gradual rise from about 150 to 350 K, indicating a continuous melting transition as

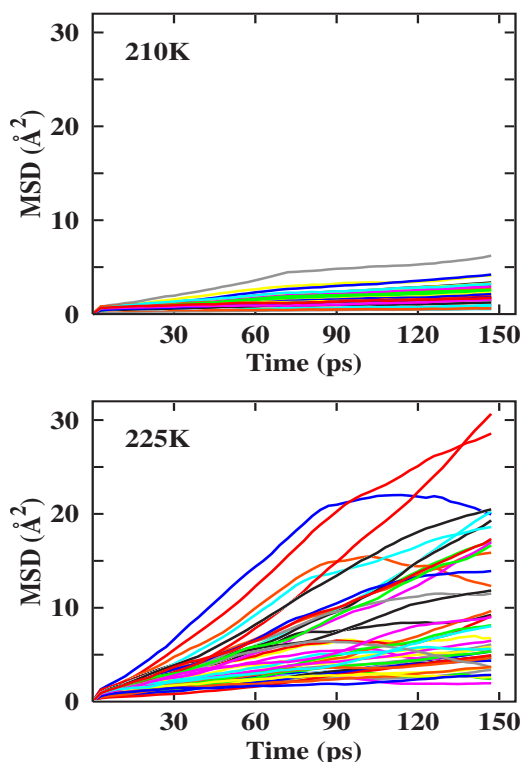


FIG. 11. (Color online) The MSDs of individual atoms calculated for  $\text{Na}_{45}$  (a) at 210 K and (b) at 225 K over the last 150 ps.

shown in Figs. 12(b) and 12(e). The shape deformation parameter  $\epsilon_{def}$  shown in Figs. 12(c) and 12(f) for both the clusters behaves differently, reflecting upon the changes in the shape of respective isomers. It may be noted that for other clusters which are relatively more ordered ( $\text{Na}_{40}$ ,  $\text{Na}_{43}$ ,  $\text{Na}_{55}$ ),  $\epsilon_{def}$  (figure not shown) remains nearly constant up to the melting region.

The systematic evolution of heat capacities can be better appreciated by examination of all the available data (calculated from density-functional simulation). In Fig. 13, we show the specific heats for all the available clusters between  $\text{Na}_{40}$  and  $\text{Na}_{55}$ . The most symmetric cluster  $\text{Na}_{55}$  shows the sharpest peak in the heat capacity. The heat capacities of  $\text{Na}_{40}$  and  $\text{Na}_{43}$  (partial icosahedral structures) have well recognizable peaks which are broader than that of  $\text{Na}_{55}$ . The disordered phase of the growth is clearly reflected in the very broad heat capacities seen around  $n=50$ .

It is interesting to correlate the energy distribution of isomers and the shape of the heat capacities. Such a relationship between the melting characteristic and the internal energy of the isomers has been brought out by Bixon and Jortner.<sup>39</sup> They showed that clusters having a large energy gap within the isomer distribution and a considerable spread of the high-lying isomers exhibit a clear transition in their caloric curve, while clusters having a continuous distribution of isomers do not exhibit such a clear melting transition. The energy isomer distribution for the first 20 isomers for representative clusters ( $n=40, 48, 52$ , and  $55$ ) is shown in Fig. 14. It can be noted that  $\text{Na}_{48}$  and  $\text{Na}_{52}$  show a continuous energy distribution, while  $\text{Na}_{40}$  and  $\text{Na}_{55}$  show energy gaps. Thus, the well

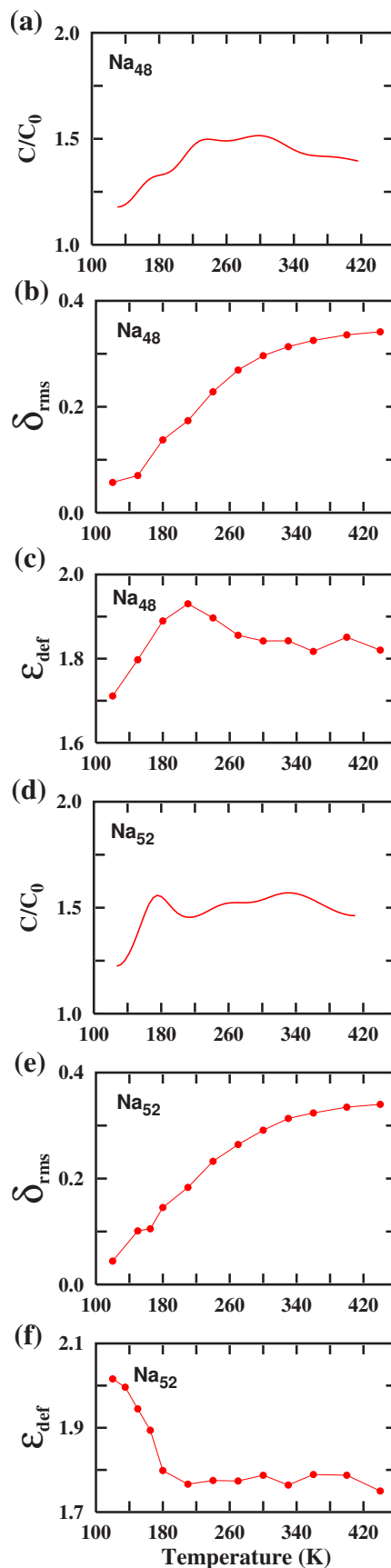


FIG. 12. (Color online) The normalized heat capacity,  $\delta_{rms}$ , and  $\epsilon_{def}$  [(a)–(c)] for  $\text{Na}_{48}$  and [(d)–(f)] for  $\text{Na}_{52}$ .

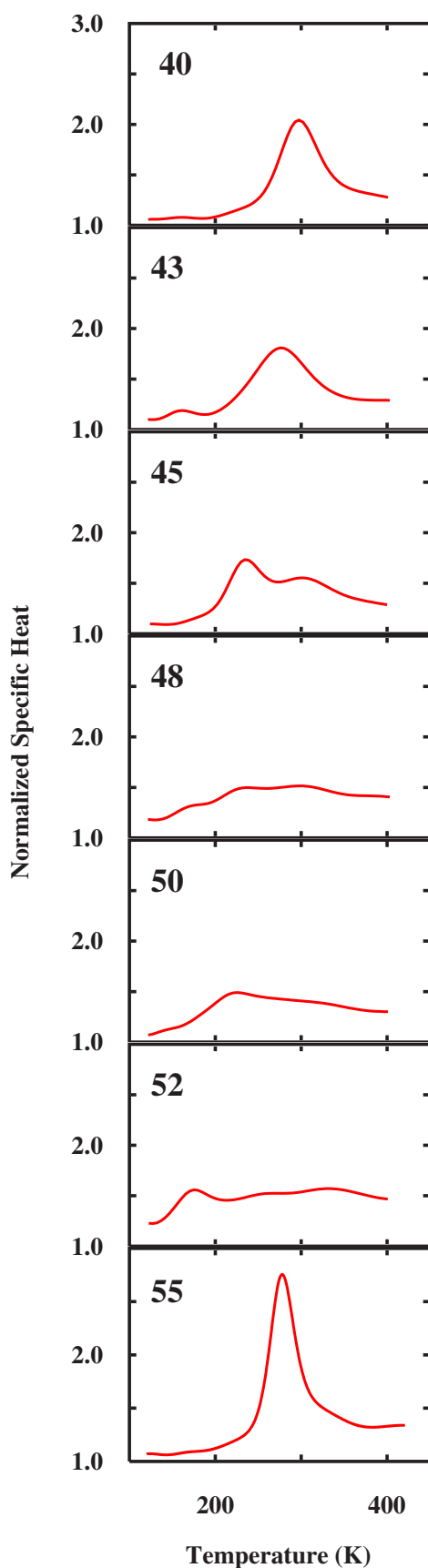


FIG. 13. (Color online) The normalized heat capacity as a function of temperature for  $\text{Na}_n$ ,  $n=40, 43, 45, 48, 50, 52$ , and  $55$ .

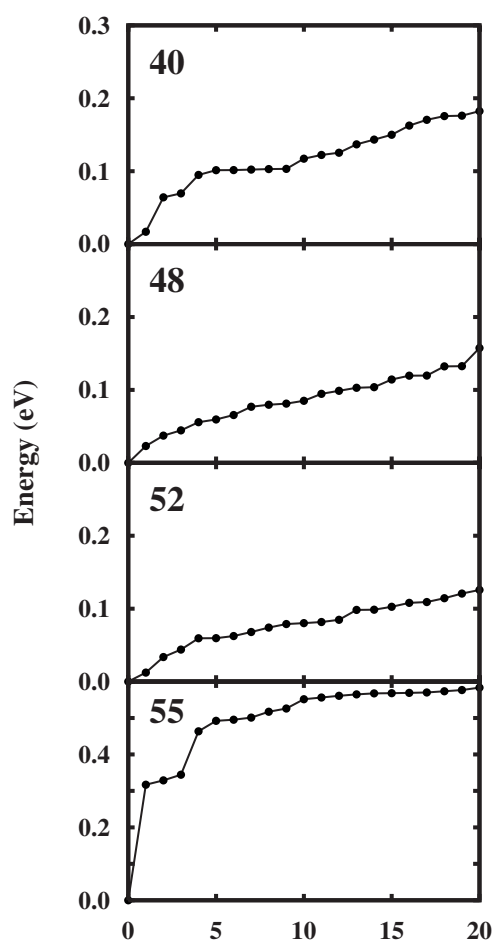


FIG. 14. The isomer energy distribution relative to ground-state energy for the first 20 isomers in  $\text{Na}_{40}$ ,  $\text{Na}_{48}$ ,  $\text{Na}_{52}$ , and  $\text{Na}_{55}$ .

ordered clusters exhibiting energy gap in the isomer distribution have well defined peaks in their heat capacity curves. It may also be noted that similar features in the heat capacity curves were also observed in the case of few other clusters using Lennard-Jones potentials.<sup>40</sup>

We have also calculated the melting temperature and latent heat for clusters that have a recognizable peaks in Table I. For the case of  $\text{Na}_{45}$ , the peak is very broad and hence we quote the upper and the lower bounds. We estimate the error of the latent heat to be of the order of 0.3 meV/atom.

TABLE I. Melting temperatures and latent heat for  $\text{Na}_n$  ( $n=40, 43, 45$ , and  $55$ ). Melting temperature is identified by the peak of the heat capacity curve.

Cluster	Melting temperature (K)	Latent heat (meV/atom)
$\text{Na}_{40}$	300	14.7
$\text{Na}_{43}$	280	16.2
$\text{Na}_{45}$	300	17.2–18.4
$\text{Na}_{55}$	280	14.0
Other clusters	Broad curve	

## V. SUMMARY AND CONCLUSION

The *ab initio* density-functional method has been applied to investigate systematic evolutionary trends in the ground-state geometries of the sodium clusters in the size range of  $n=39-55$ . The DFMD finite-temperature simulations have been carried out for representative clusters. A detailed comparison between the heat capacities and the geometries firmly establishes a direct influence of the geometries on the shapes of the heat capacity curves. The heat capacities show size sensitivity. The growth pattern shows a transition from ordered  $\rightarrow$  disordered  $\rightarrow$  ordered sequence.

The corresponding heat capacities show a transition from peaked to a very broad to peaked sequence. It is seen that addition of a few atoms changes the shape of heat capacity very significantly. We believe that the size-sensitive feature

seen in our simulation is universal. It may be noted that such a feature has been observed experimentally in the case of gallium and aluminum and in the case of DFMD simulations for gold. We await the experimental measurements of the heat capacities on the sodium clusters in this range showing the size sensitivity.

## ACKNOWLEDGMENTS

We acknowledge partial assistance from the Indo-French Center for Promotion of Advance Research (India)/Center Franco-Indian pour la Promotion de la Recherche Avancée (France) (IFC-PAR, Project No. 3104-2). We would like to thank Kavita Joshi and Sailaja Krishnamurty for a number of useful discussions.

- 
- <sup>1</sup>P. G. Reinhard and E. Suraud, *Introduction to Cluster Dynamics* (Wiley-VCH, Berlin, 2003).
- <sup>2</sup>M. Schmidt, R. Kusche, B. von Issendorff, and H. Haberland, *Nature (London)* **393**, 238 (1998); R. Kusche, Th. Hippler, M. Schmidt, B. V. Issendorff, and H. Haberland, *Eur. Phys. J. D* **9**, 1 (1999); M. Schmidt, R. Kusche, Th. Hippler, J. Donges, W. Kronmüller, B. von Issendorff, and H. Haberland, *Phys. Rev. Lett.* **86**, 1191 (2001); M. Schmidt and H. Haberland, *C. R. Phys.* **3**, 327 (2002).
- <sup>3</sup>M. Schmidt, J. Donges, Th. Hippler, and H. Haberland, *Phys. Rev. Lett.* **90**, 103401 (2003).
- <sup>4</sup>H. Haberland, Th. Hippler, J. Donges, O. Kostko, M. Schmidt, and B. von Issendorff, *Phys. Rev. Lett.* **94**, 035701 (2005).
- <sup>5</sup>Y. Li, E. Blaisten-Barojas, and D. A. Papaconstantopoulos, *Phys. Rev. B* **57**, 15519 (1998).
- <sup>6</sup>F. Calvo and F. Spiegelmann, *Phys. Rev. Lett.* **82**, 2270 (1999).
- <sup>7</sup>F. Calvo and F. Spiegelmann, *J. Chem. Phys.* **112**, 2888 (2000).
- <sup>8</sup>F. Calvo and F. Spiegelmann, *J. Chem. Phys.* **120**, 9684 (2004).
- <sup>9</sup>J. A. Reyes-Nava, I. L. Garzón, M. R. Beltrán, and K. Michaelian, *Rev. Mex. Fis.* **48**, 450 (2002); J. A. Reyes-Nava, I. L. Garzón, and K. Michaelian, *Phys. Rev. B* **67**, 165401 (2003).
- <sup>10</sup>K. Manninen, A. Rytönen, and M. Manninen, *Eur. Phys. J. D* **29**, 39 (2004).
- <sup>11</sup>A. Rytönen, H. Häkkinen, and M. Manninen, *Phys. Rev. Lett.* **80**, 3940 (1998).
- <sup>12</sup>A. Rytönen, H. Häkkinen, and M. Manninen, *Eur. Phys. J. D* **9**, 451 (1999).
- <sup>13</sup>K. Manninen, H. Häkkinen, and M. Manninen, *Phys. Rev. A* **70**, 023203 (2004); K. Manninen, T. Santa-Nokki, Häkkinen, and M. Manninen, *Eur. Phys. J. D* **34**, 43 (2005); K. Manninen, H. Häkkinen, and M. Manninen, *Comput. Mater. Sci.* **35**, 158 (2006).
- <sup>14</sup>S. Chacko, D. G. Kanhere, and S. A. Blundell, *Phys. Rev. B* **71**, 155407 (2005).
- <sup>15</sup>M.-S. Lee, S. Chacko, and D. G. Kanhere, *J. Chem. Phys.* **123**, 164310 (2005).
- <sup>16</sup>A. Aguado and J. M. López, *Phys. Rev. Lett.* **94**, 233401 (2005).
- <sup>17</sup>A. Aguado and J. M. López, *Phys. Rev. B* **74**, 115403 (2006).
- <sup>18</sup>M. Itoh, V. Kumar, and Y. Kawazoe, *Phys. Rev. B* **73**, 035425 (2006).
- <sup>19</sup>O. Kostko, B. Huber, M. Moseler, and B. von Issendorff, *Phys. Rev. Lett.* **98**, 043401 (2007).
- <sup>20</sup>M.-S. Lee and D. G. Kanhere, *Phys. Rev. B* **75**, 125427 (2007).
- <sup>21</sup>G. A. Breaux, D. A. Hillman, C. M. Neal, R. C. Benirschke, and M. F. Jarrold, *J. Am. Chem. Soc.* **126**, 8628 (2004).
- <sup>22</sup>K. Joshi, S. Krishnamurty, and D. G. Kanhere, *Phys. Rev. Lett.* **96**, 135703 (2006).
- <sup>23</sup>G. A. Breaux, C. M. Neal, B. Cao, and M. F. Jarrold, *Phys. Rev. Lett.* **94**, 173401 (2005).
- <sup>24</sup>S. Krishnamurty, G. Shafai, D. G. Kanhere, B. Soule de Bas, and M. J. Ford, *J. Phys. Chem. A*, 10.1021/jp075896 (2007).
- <sup>25</sup>U. Röthlisberger and W. Andreoni, *J. Chem. Phys.* **94**, 8129 (1991).
- <sup>26</sup>I. A. Solov'yov, A. V. Solov'yov, and W. Greiner, *Phys. Rev. A* **65**, 053203 (2002).
- <sup>27</sup>A. Aguado, J. M. Lopez, J. A. Alonso, and M. J. Stott, *J. Chem. Phys.* **111**, 6026 (1999).
- <sup>28</sup>A. Aguado, J. M. Lopez, J. A. Alonso, and M. J. Stott, *J. Phys. Chem. B* **105**, 2386 (2001).
- <sup>29</sup>The angular momentum is removed periodically; A. Vichare, D. G. Kanhere, and S. A. Blundell, *Phys. Rev. B* **64**, 045408 (2001).
- <sup>30</sup>M. C. Payne, M. P. Teter, D. C. Allan, T. A. Arias, and J. D. Joannopoulos, *Rev. Mod. Phys.* **64**, 1045 (1992).
- <sup>31</sup>D. Vanderbilt, *Phys. Rev. B* **41**, 7892 (1990).
- <sup>32</sup>Vienna *ab initio* simulation package (VASP), Technische Universität Wien, 1999; G. Kresse and J. Furthmüller, *Phys. Rev. B* **54**, 11169 (1996).
- <sup>33</sup>Z. Li and H. A. Scheraga, *Proc. Natl. Acad. Sci. U.S.A.* **84**, 6611 (1987); D. J. Wales and J. P. K. Doye, *J. Phys. Chem. A* **101**, 5111 (1997).
- <sup>34</sup>M. Iwamatsu, *J. Chem. Phys.* **112**, 10976 (2000).
- <sup>35</sup>J. A. Niesse and H. R. Mayne, *J. Chem. Phys.* **105**, 4700 (1996).
- <sup>36</sup>R. G. Parr and W. Yang, *The Density Functional Theory of Atoms and Molecules* (Oxford University Press, New York, 1989).
- <sup>37</sup>A. M. Ferrenberg and R. H. Swendsen, *Phys. Rev. Lett.* **61**, 2635 (1988).
- <sup>38</sup>P. Labastie and R. L. Whetten, *Phys. Rev. Lett.* **65**, 1567 (1990).
- <sup>39</sup>M. Bixon and J. Jortner, *J. Chem. Phys.* **91**, 1631 (1989).
- <sup>40</sup>D. D. Frantz, *J. Chem. Phys.* **102**, 3747 (1995).